論文

A Study on Microfailure Mechanism of Single-Fiber Composites using Tensile/Compressive Broutman Fragmentation Techniques and Acoustic Emission

Joung-Man Park*, Jin-Won Kim** and Dong-Jin Yoon***

인장/압축 Broutman Fragmentation시험법과 음향방출을 이용한 단섬유 복합재료의 미세파괴 메커니즘의 연구

박종만*, 김진원**, 윤동진***

초 록

탄소섬유/에폭시 복합재료의 계면 및 미세파괴 물성을 인장 fragmentation과 압축 Broutman 두 시험법과 음향방출 시험을 이용하여 평가하였다. Maleic anhydride polymeric coupling agent와 amino-silane를 각각 전기증착법 및 dipping을 통하여 섬유표면에 적용하였다. 두 coupling agents를 사용한 섬유와 기지간의 계면전단강도는 인장 및 압축 두 시험에서 모두 미처리와 비교하여 큰 증가를 나타내었다. 인장시험 동안에, 원추모양의 섬유파단과 기지의cracking 그리고 부분적인 interlayer failure로 이루어진 전형적인 미세파괴 형태가 발생하였다. 이에 비하여, 압축시험에서는 부러진 섬유의 끝에서 대각선 방향이 슬립거동이 관찰되었다. 주어진 두 힘의 하중상태에서 섬유의 파단은 항복점 전후 부근에서 일어났다. 음향방출분포는 인장에서 섬유표면 처리와 미처리의 두 조건에서 미세파괴 신호가 잘 분리되었으며, 한편, 압축에서는 signal이 다소 중복되어 나타났다. 이는 탄소섬유의 인장력/압축력 간의 파괴에너지 차이에 기인한다고 고려된다. 탄소와 basalt 섬유복합재료의 섬유파단 waveform의 최대 voltage는 압축보다 인장시험에서 상당히 크게 나타났으며, 이들은 음향방출시험으로 파괴에너지 차이를 명확히 비교 및 확인할 수 있었다.

ABSTRACT

Interfacial and microfailure properties of carbon fiber/epoxy matrix composites were evaluated using both tensile fragmentation and compressive Broutman tests with an aid of acoustic emission (AE) monitoring. A polymeric maleic anhydride coupling agent and a monomeric amino-silane coupling agent were used via the electrodeposition (ED) and the dipping applications, respectively. Both coupling agents exhibited significant improvements in interfacial shear strength (IFSS) compared to the untreated case under tensile and compressive tests. The typical microfailure modes including fiber break of cone-shape, matrix cracking, and partial interlayer failure were observed during tensile test, whereas the diagonal slippage in fiber ends was observed under compressive test. For both loading types, fiber breaks occurred

* 경상대학교 응용화학공학부/고분자공학전공, 항공기부품기술연구센타
** 경상대학교 대학원 고분자공학과
*** 한국표준과학연구원 방재기술센타 비파괴평가그룹

around just before and after yielding point. In both the untreated and treated cases AE amplitudes were separately distributed for the tensile testing, whereas they were closely distributed for the compressive tests. It is because of the difference in failure energies of carbon fiber between tensile and compressive loading. The maximum AE voltage for the waveform of carbon or basalt fiber breakages under tensile tests exhibited much larger than those under compressive tests, which can provide the difference in the failure energy of the individual failure processes.

INTRODUTION

Interfacial properties between fiber and matrix are very important to control the mechanical performance in composite materials. The single-fiber pullout test [1] and single-fiber composite (SFC) test (also known as the fragmentation test) [2], have been commonly used for characterizing the fiber-matrix interfacial properties under tensile loading [3-4] in addition to microindentation test under compressive loading [5]. The single-fiber pullout test (which is also known as the microdroplet test [1,3]) can measure the interfacial shear strength (IFSS) by pulling out a fiber from a lump of the polymer matrix. In the microindentation test, a rigid indentor is pushed down on a cross-sectional area of the fiber in a thin real composite plate. Latter two tests are essentially similar in a point of view that the IFSS can be detected directly. The SFC test, originally proposed by Kelly-Tyson [2] for metal matrix composites, can provide abundant statistical information using only several specimens as well as the microfailure modes and IFSS.

Recently the single-fiber Broutman test was investigated the fiber-matrix interface debonding behavior by subjecting to a transverse tensile load with an aid of acoustic emission (AE) [6]. Marom *et al.* [7-9] studied the compressive fragmentation phenomenon using microcomposites to evaluate thermal stresses, single-fiber compressive strengths, Weibull parameters and IFSS. A compressive fragmentation test, using thermal stresses, was developed to determine the compressive strengths and Weibull parameters to characterize the strength-length dependence of carbon fibers. Transverse interfacial properties of the fiber/matrix were studied by the single-fiber Broutman test to investigate the interfacial debonding and buckling behavior while subjecting to a compressive stress.

IFSS can be improved by an introduction of chemical functional groups to the fiber surface via electrolytic oxidation [10], ammonia plasma treatment [11] or coupling agent applications [12,13]. Among them is the electrodeposition (ED) [14-16], which is a process that a film is deposited on a conductive surface (such as carbon fiber) from a dispersion of colloidal ions in water with a charge opposite to that of the carbon fiber surface. By optimizing the process, a polymeric coating can be deposited with the desire composition and thickness homogeneously to improve the interfacial properties.

AE is well known as one of the important nondestructive testing methods. The AE can monitor the fracture behavior of a composite structure, and characterize AE parameters in order to understand the type of fractures sources and their progressing [17-20]. When the tensile/compressive loading is applied to a composite material, AE signal may occur from fiber fracture, matrix cracking, and debonding at the fiber-matrix interface. The AE energy released by fiber fracture should be greater than that associated by debonding or matrix cracking.

In this work, interfacial properties of the ED or the dipping treated carbon fiber/epoxy matrix composites are evaluated using both the tensile and compressive fragmentation tests. During the

Table 1. Chemical structures of two coupling agents

Chemical Name	Chemical Structure
Polybutadiene maleic anhydride (PBMA)[1]	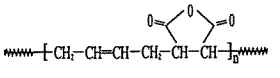
3-Aminopropyltrimethoxysilane (APS)[2]	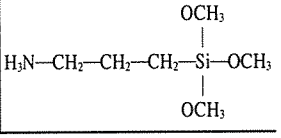

1) Polymeric type (Polyscience Inc.)
2) Monomeric type (Aldrich Chemical Inc.)

tests, AE signals of microfailure sources are monitored to study their correlation with the IFSS.

EXPERIMENTAL

Materials

Carbon fiber (Tae Kwang Co., TZ-307) has a density of 1.8 g/㎤ and average diameter of 7.9 ㎛, whereas tensile strength and modulus are 3727 MPa and 245 GPa, respectively. Basalt fiber having 98㎛ in diameter, which was made from naturally occurring basalt rock in the Washington state area, U.S.A. was used for comparing the diameter effect. A polymeric coupling agent (polybutadiane-maleic anhydride (PBMA)) was used for ED on the carbon fiber surface, and was totally soluble in the deionized water. A monomeric silane coupling agent including amino-functional groups, γaminopropyl triethoxysilane (APS), was used for carbon and basalt fibers for the dipping application. Their chemical structures are shown in Table 1.

Epoxy resin (YD-128, Kukdo Chemical Co.) as matrix is based on diglycidylether of bisphenol-A (DGEBA), and Jeffamine D400 (Huntsman Petrochemical Co.) based on polyoxypropylenediamine was used as a curing. It was precured for 2 hours at 80 ℃ and then postcured for 2 hours at 120 ℃.

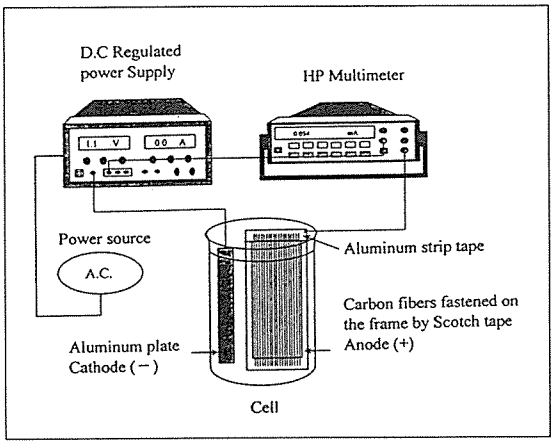

Fig. 1. Schematic plot of electrodeposition (ED) system

Methodologies

Measurement of Single-Fiber Strength: Tensile strength of single-carbon fiber was obtained using about fifty specimens for statistical mean value. Average diameter of forty fibers was measured by an optical microscope attached a calibrated eye' s piece. Single fiber was placed in the centerline on the middle of a paper frame, and fixed the fiber using Scotch tapes, and then finally glued the fiber using an epoxy adhesive. Universal testing machine (UTM) (LR-10K, Lloyd Instrument Ltd.) was used to measure the single-fiber tensile strength. Load cell was 100 N being a small capacity, and the crosshead speed was 0.5 mm/minute.

Fiber Surface Treatment by ED and Dipping: Coupling agents were diluted to the 0.5 wt% concentration in aqueous solution. Conductive carbon fiber was modified via both ED and the dipping treatments, whereas non-conductive basalt fiber was treated by only the dipping method. The carbon fibers acted as an anode in itself whereas the cathode was made of an aluminum plate. PBMA coupling agents were diluted to the suitable concentration in the deionized water as shown in figure 1. After anode frame and cathode bar was immersed into aqueous elec-

trolyte solutions, voltage was supplied to both electrodes by power source. Typical immersing time and applied voltage were 10 minutes and 3 Voltages, respectively. APS coupling agent was diluted to the required 0.5 wt.% concentration in aqueous solution for coating on carbon or basalt fiber surface for comparison, respectively.

Preparation Tensile/Compressive Microspecimens: Tensile and compressive Broutman microspecimens were made of single-fiber embedded in epoxy matrix in silicone mould as shown in figure 2. Tensile specimen is dog-bone-shaped, whereas compressive specimen is curved neck-shaped, where a fiber is laid longitudinally. The application of a compressive load to the curved neck-shaped specimen results in large compressive stress in the smallest cross-section. It in turn causes Poisson's expansion in the transverse direction. As the Poisson's ratio of the matrix is larger than that of the fiber, the transverse expansion of the matrix is larger than that of the fiber and a transverse debonding stress is induced at the interface. Debonding occurs in the middle of the specimen where the transverse stress at the fiber ends [6].

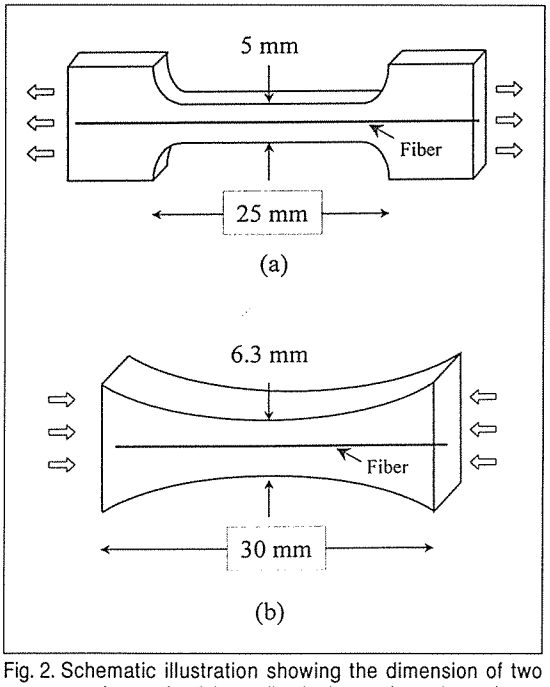

Fig. 2. Schematic illustration showing the dimension of two specimens for (a) tensile dogbone-shaped specimen; and (b) compressive curved neck Broutman specimen

Tensile/Compressive IFSS Measurements: The fragmentation test to obtain IFSS was carried out using UTM. Ultimate fragment lengths were measured, and subsequent failure process was observed via a polarized-light microscope. Tensile specimens were tested tensilely by universal testing machine (10 kN load cell, 0.25 mm/minute crosshead speed rate). On the other hand, the compressive test was performed with a crosshead speed of 2 mm/minute for carbon fiber and 1 mm/minute for basalt fiber specimens, based on two fiber's tensile properties, with AE monitoring. Their stress-strain curves were drawn. The relationship among fiber tensile strength σ_f, aspect ratio l_c/d, and tensile IFSS, τ_t was given by Kelly-Tyson equation [2,18] as,

$$\tau_t = \frac{\sigma_{fu} \cdot d}{2\bar{l}_c} \tag{1}$$

where σ_{fu} is the tensile strength of the fiber at average critical length $\bar{l}_c$, and d is the fiber diameter. On the other hand, the compressive stress of the fiber can be transferred across the break portion from one fiber fragment to the other. It is due to the fact that the fragments are still in contact with each other. A critical fragment length, as defined by the tensile load transfer model, does not exist in compressive loading system [7]. According to the compressive stress profile, compressive IFSS, τ_c is also based on the force balance,

$$\tau_c = \frac{\sigma_{fc} \cdot d}{2\bar{l}_c} \tag{2}$$

where average critical length $\bar{l}_c$ is the fiber

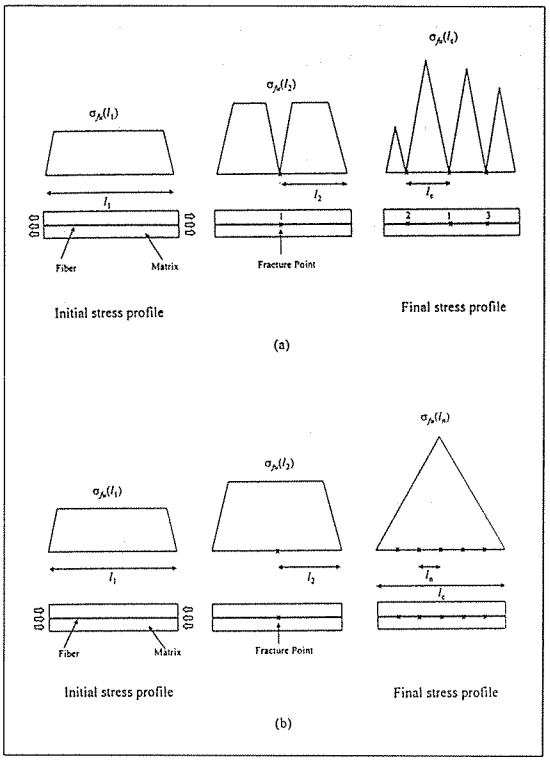

Fig. 3. Schematic diagram of stress profile with increasing loading condition for (a) tensile and (b) compressive systems

length ($\overline{l_c} = l_1$) at pure shear region around center. σ_{fc} is the fiber stress at the point where the interfacial stress is insufficient to induce further fragmentation.

Figure 3 shows schematic diagrams of stress profile under increasing loading condition: (a) tensile and (b) compressive tests. In figure 3(a), Kelly-Tyson model assumes that the tensile stress in the fiber builds up from the broken fiber ends and that the fragmentation occurs when the built stress in the fiber reaches the fiber tensile strength. As the tensile stress was applied further, the fiber fracture process continued until no longer fracture occurred in the fiber. At this strain a fragment length is called as a critical fragment length, l_c. The critical fragment length of the individual fiber was measured and their microfailure modes were observed via a polarized-light microscope.

In compressive test in figure 3(b), unlike in tension, the fiber fragmentation does not result in a stress discontinuity at the point of fiber fracture, because the fiber fragments remain in contact and can still bear a compressive load, i.e., the stress state around the center region of the original fiber remains constant and equal to the compressive stress on the fiber [7].

Fiber strength can be calculated from the extrapolation gauge length using Weibull weakest link rule [21,22]. The fiber strength σ_f at the critical fragment length is

$$\sigma_f = \sigma_{f0} \cdot \left(\frac{\overline{l_c}}{l_0} \right)^{-\frac{1}{\beta}} \tag{3}$$

where σ_{f0} is fiber strength at gauge length, l_0, $\overline{l_c}$ is average fragment length, and β is shape parameter of the Weibull distribution for the fiber strength.

AE Measurement: Micro-specimen was placed on the UTM for tensile/compressive tests. AE sensor was attached in the center of the specimen using vacuum grease couplant. AE signals were detected using a miniature sensor (Resonance Type model, PICO by PAC) with peak sensitivity of 54 Ref V/(m/s) and resonant frequency at 500 kHz. The sensor output was amplified by 40 dB at preamplifier and passed through a band-pass filter with a range of 200 kHz to 750 kHz. The threshold level was set up as 30 dB. Then the signal was fed into an AE signal process unit (MISTRAS 2001 system), where AE parameters were analyzed using in-built software. Typical AE parameters such as hit rate, peak amplitude, and event duration were investigated for the time and the distribution analysis. Schematic diagram of AE system is shown in figure 4.

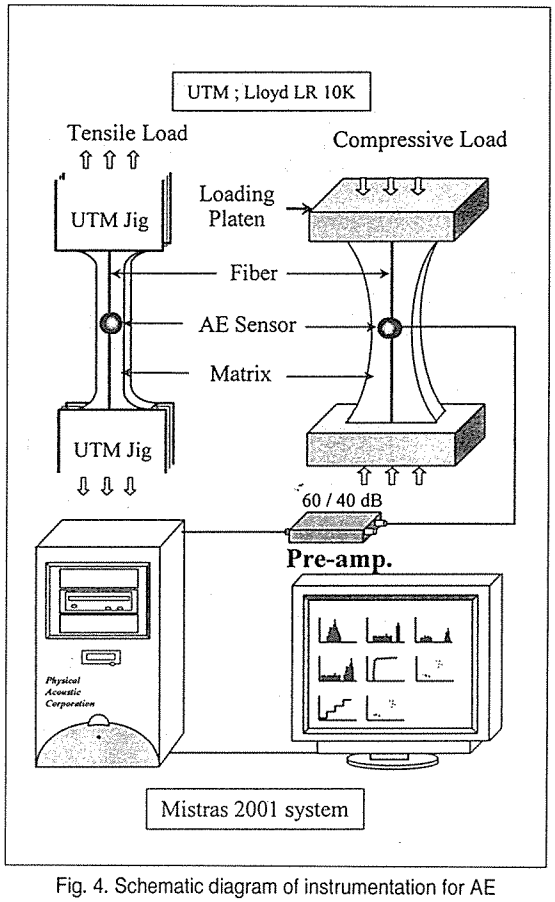

Fig. 4. Schematic diagram of instrumentation for AE

RESULTS and DISCUSSION

Mechanical Properties of Untreated/ Treated Carbon Fibers

Table 2 shows the tensile and the compressive strength properties for the untreated and the treated carbon fibers. Tensile strength of the treated carbon fiber was improved significantly than the untreated fiber, with exhibiting the similar value for both the ED and the dipping treatments. Direct measurement of the compressive strength requires the experimental difficulty. Carbon fiber appeared to have compressive strength to tensile strength ratios of 10-30 % for high moduli having with the

Table 2. Properties of carbon fiber with two types of the fiber treatment under tensile and compressive loading

Types	No. of Specimen (EA)	Diameter (μm)	Scale Parameter (α)	Shape Parameter (β)	Tensile Strength (MPa)[2]	Compressive Strength (MPa)[3]
Untreated	49	7.9 (0.1)[1]	3971	5.44	3664 (716)	2432
ED	44	8.9 (0.3)	4488	5.31	4458 (721)	2960
Dipping	40	8.2 (0.4)	4865	4.70	4722 (953)	3135

1) Standard deviation (SD)
2) Gauge length of specimens: 2 mm
3) Calculated from Ref. (7)

range of 380-480 GPa [23], where the compressive strength is remarkably low. On the other hands, the ratio of the compressive strength to tensile strength for a low modulus carbon fiber in the range of 260 GPa by the transverse tensile test was found to be 66.4 % by Wagner *et al.* [9].

Compressive strength of carbon fiber in this work was calculated from 66.4 % of the measured tensile strength value because used carbon fiber modulus was 245 GPa from the latter case. Tensile strength of carbon fiber by the dipping exhibited the highest improvement, due to the healing effect of the fiber flaw in addition to the wetting effect. The reason for rather decreasing tensile strength for ED treatment compared to the dipping is considered to be intensely compact packing on fiber surface by ionized electrolyte.

Microfailure Modes and Comparison of IFSS

In compressive test, the original stress profile along the fiber is entirely unchanged by the fiber fracture, since as the first approximation the compressive stress can be transferred across the break portion from one fiber fragment to the other. As the compressive stress on the fiber increases further, the fiber may break again at a stress corresponding to the larger compressive strength of the new smaller fragment length in accordance with

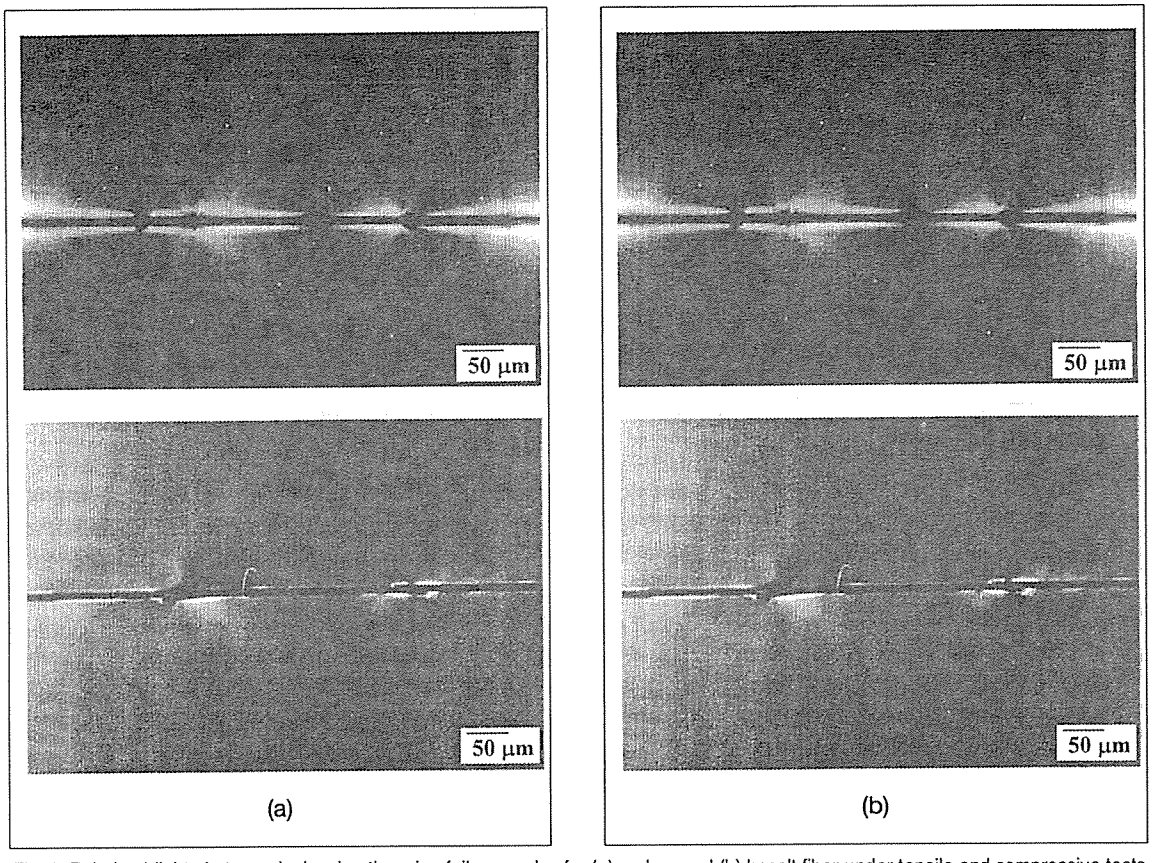

Fig. 5. Polarized-light photograph showing the microfailure modes for (a) carbon and (b) basalt fiber under tensile and compressive tests

the strength-length dependence, i.e., Weibull weakest link rule. An increase in applied strain on the specimen may not result in an increase in the stress on the fiber and hence the fragment length may remain constant. The stress transfer length increases concomitantly at both fiber ends. Unlike in the tensile fragmentation the average fragment length at this point is not related to a critical length as the conventional tensile load transfer model.

The curved-neck specimen under longitudinal compression causes interface debonding to occur in the transverse direction (i.e., tensile debonding) due to the transverse expansion of the matrix when its Poisson' s ratio is greater than that of the fiber. The single-fiber compressive test has been not so useful as other tensile microcomposite tests because of the problems associated with the difficulties in the specimen preparation and in the visual detection of the onset of interfacial debonding. The fibers should be aligned accurately for reproducible results.

Figure 5 shows the photographs of microfailure modes for (a) carbon fiber and (b) basalt fiber under tensile and compressive tests. In figure 5(a), carbon fiber fracture under tensile test occurred with cone-shaped and stress whitening was observed around fiber break portion, whereas in compressive test the diagonal slippage were observed based on transverse tensile stress, which is characteristic of the transverse properties of the interface. In figure 5(b) large basalt fiber fracture

Table 3. The aspect ratio and IFSS improvement for ED and the dipping applications under tensile and compressive tests

Types		Aspect Ratio (l_c/d)	Fiber Strength (MPa)[1)]	IFSS	Improvement (%)
Tensile	Untreated	71.6	5031	35.1	–
	ED	59.7	6575	55.1	57.0
	Dipping	65.2	6488	49.8	32.6
Compressive	Untreated	35.8	3328	1.29	–
	ED	24.3	4469	1.99	54.2
	Dipping	34.6	4752	2.02	56.6

1) Fiber Strength of critical fragment length, l_c

was observed with diagonal stress whitening distribution in addition to the initial cone-shaped matrix cracking in tensile test. On the other hand, in compressive test basalt fiber composites exhibited large sized diagonal slippage coming from fiber fracture in center region of the specimen. Stress whitening was also observed around the fiber slippage, which results in the debonding propagation.

Table 3 shows the aspect ratio and IFSS improvement for ED and the dipping applications under tensile and compressive tests. IFSS by ED and the dipping applications showed high improvement compared to the untreated case under both tensile and compressive tests. Since IFSS is a function of aspect ratio and fiber strength at critical fragment length, the final IFSS by the ED and the dipping exhibited higher than that of the untreated. Fiber strength value, l_c was obtained using the Weibull weakest link rule by extrapolating the fiber strength at critical fragment length. Not unexpectedly, IFSS of compressive test appeared much lower than IFSS of tensile test. The value of 1-2 MPa is much lower than the shear yield strength of the used epoxy matrix (about 70 MPa at 25 ℃). That is to say that interfacial debonding failure occurred rather than shear yielding of the epoxy matrix.

Both two coupling agents exhibited significant improved IFSS compared to the untreated case

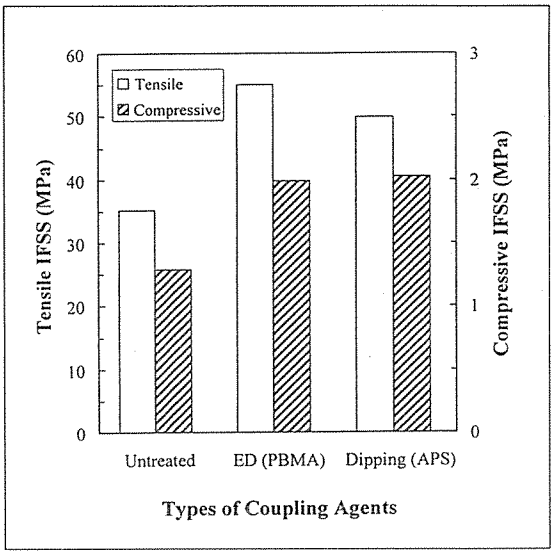

Fig. 6. IFSS for two coupling agents compared to the untreated case

under both tensile and compressive tests as shown in figure 6. It may be due to the primary and the secondary chemical bonding as well as physical interdiffusion between coupling agents and epoxy matrix, respectively. In the tensile test ED treated specimen exhibited higher IFSS improvement than the dipping by APS coupling agent. It may be because better wetting due to polymeric nature and more uniform coating can contribute to affect IFSS favorably. On the other hand, the compressive test appeared the comparative IFSS improvement for ED and the dipping applications unlike the case of the tensile test. It may be because of the compensative effectiveness on the IFSS contributing as functions of the aspect ratio meaning the stress transfer mechanism and the compressive fiber strength at critical fiber fragment length. It may also be because the carbon fiber' s fracture energy between the tensile and the compressive tests can be different from each other, as shown in the next AE results. Under tensile load, carbon fiber is known to fail due to the strong covalent bonding, whereas the fiber can fail due to rather less strong secondary or van der Waals bonding

under compressive loading.

In general, two microfailure mechanisms can appear to be competitive in the compressive Broutman test, i.e. fiber breaking under compressive stresses and fiber-matrix interface transverse debonding [6]. The first, when the fiber-matrix interface bonding is high, fiber fracture occurred in advance. It is because the compressive stress in the specimen exceeded the fiber compressive strength prior to the transverse debonding stress exceeded the IFSS. The result reflects the shear properties of the interface. The second, when the interfacial transverse strength is not so high, the interfacial debonding under transverse stresses occur first. The result can be characteristic of the transverse properties of the interface.

AE Analysis with Microfailure Mechanisms

Figure 7 shows the microfailure mechanisms for carbon and basalt fiber/composites with stress-strain curves using the tensile and the compressive tests. AE amplitudes are separated well in tensile tests for both the untreated and the treated cases in carbon and basalt fiber composites, whereas they are rather closely distributed in compressive tests. Fracture energy in tensile failure may be much higher than the case in compressive test. Especially, almost 20 dB differences were observed in

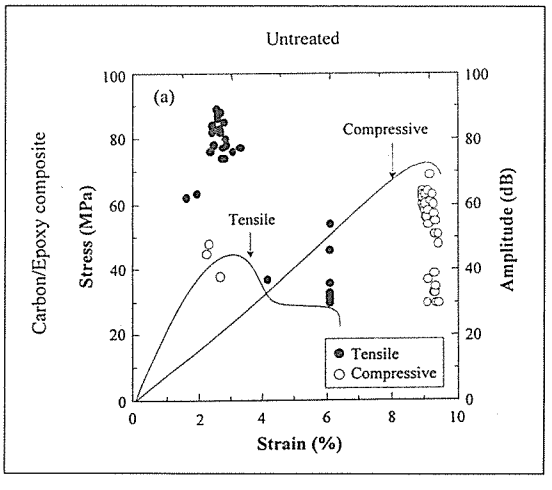

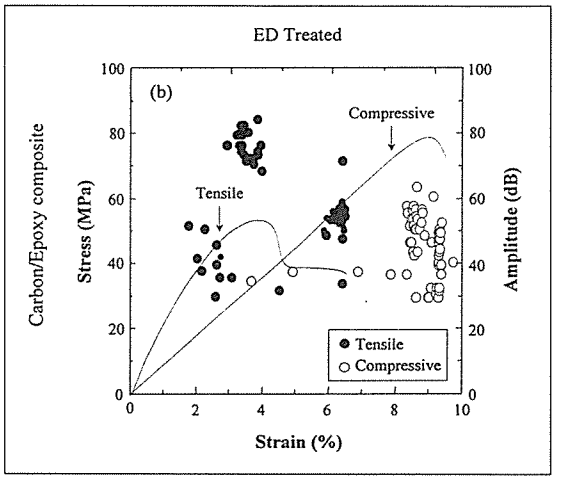

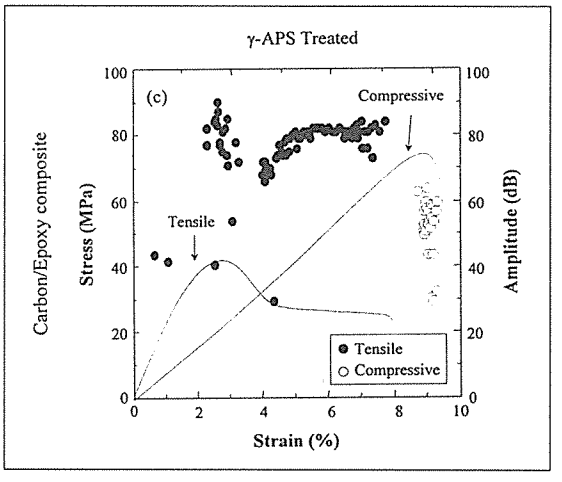

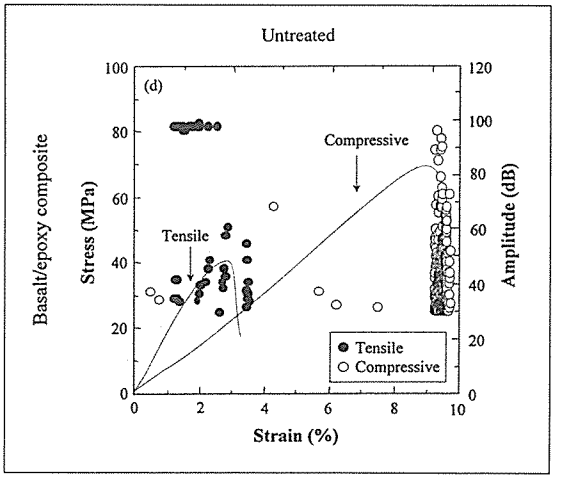

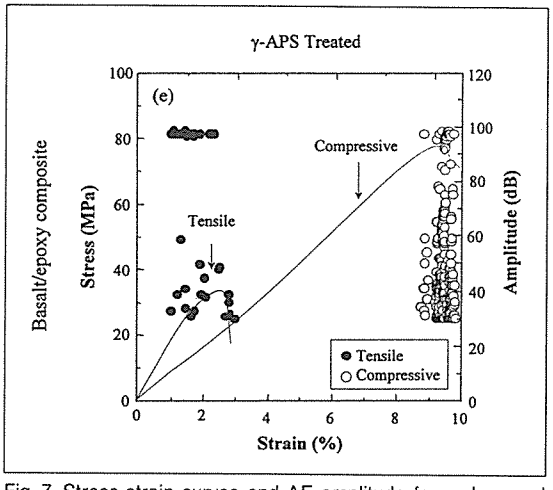

Fig. 7. Stress-strain curves and AE amplitude for carbon and basalt fiber/epoxy composites using tensile and compressive tests: (a) the untreated-; (b) ED treated-; (c) 0.5 wt.% APS treated carbon fiber; (d) the untreated-, and (e) 0.5 wt.% APS treated basalt fiber

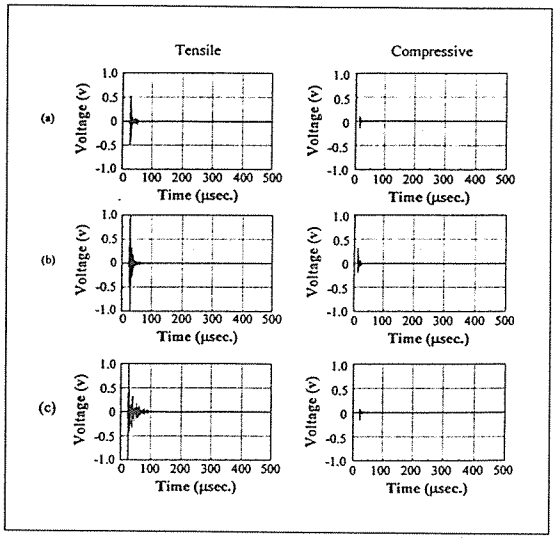

Fig. 8. AE waveform in carbon fiber/epoxy composites: (a) the untreated; (b) ED treated; and (c) 0.5 wt.% APS treated carbon fiber fracture signal under tensile and compressive tests

case of the carbon fiber fracture. It is probably because of the difference in fracture energies between the longitudinal tensile loading in tensile test and the transverse tensile loading in compressive test. For both untreated and treated cases, carbon and basalt fiber breaks occurred until just before yielding point under tensile test. Beyond yielding point, however, much more AE events occurred from the interlayer failure in both the ED and APS treated carbon cases, whereas basalt fiber composite exhibited matrix and interlayer failure around before and just after yield point. Ultimate stress in compressive test exhibited much higher than that of tensile test. All microfailures including fiber break, matrix cracking, and interlayer fracture can be correlated with their inherent material properties. Basalt fiber composites exhibited significantly higher amplitudes (about 100 dB) than those of the carbon fiber composites (70-90 dB range) due to higher fracture occurring from thicker fiber under tensile and compressive tests.

Figure 8 shows AE waveforms in (a) the untreated, (b) ED treated and (c) APS treated carbon fiber/epoxy composites. In the case of tensile fragmentation test, there were so many waveforms with intermediate amplitude coming from the interlayer failure in the treated conditions. In case of compressive Broutman test, the interlayer failure signal with the intermediate waveform overlapped with carbon fiber fracture signals. The maximum AE voltages coming from the carbon fiber break waveform under tensile tests were much larger than those under compressive tests. Under tensile test ED and APS treated carbon fiber waveform exhibited larger than the untreated case. In compressive test the waveform of ED treated carbon fiber exhibited larger voltage than the untreated case and even than APS treated case. It may be due to the microfailure types and differing failure energies in compressive tests for both the untreated and the treated carbon fibers.

Figure 9 shows AE waveform of the untreated and APS treated basalt fiber/epoxy composites. Tensile fracture signal of basalt fiber showed much larger voltage than the case of compressive test, as in the carbon fiber composites. Not unex-

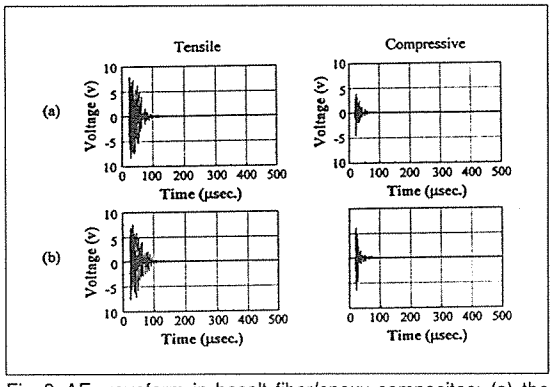

Fig. 9. AE waveform in basalt fiber/epoxy composites: (a) the untreated; (b) 0.5 wt.% treated basalt fiber fracture signal under tensile and compressive tests

pectedly, signal size of basalt fiber fracture was much larger than that of carbon fiber fracture, due to much larger diameter. There were no significant differences in signal size between the untreated and APS treated cases. Especially, interlayer failure waveforms were not observed unlike the carbon fiber case. Matrix signal was hard to distinguish from the debonding signal because of the overlapped outcome based on similar energy range.

CONCLUSIONS

Using tensile fragmentation and compressive Broutman tests, interfacial properties including IFSS were investigated by using polymeric PBMA via ED and monomeric APS coupling agents via the dipping applications. Both ED and the dipping treatments exhibited significantly improved IFSS compared to the untreated case, in addition to ED appeared higher IFSS than the dipping application in the tensile test. It may be due to the interlayer with the compact and more uniform surface coating in ED case. In compressive test for carbon and basalt fiber composites, there were diagonal slippages based on the characteristic of the transverse tensile stress in the interface. AE test monitored the signals of microfailure, such as fiber break, matrix cracking, especially diagonal slippage in the broken fiber ends. Fracture energy difference of carbon fiber between under tensile and compressive tests as well as differing diameter effect were identified by means of AE due to each differing fracture energy, respectively.

For both the untreated and the treated cases AE events were separated well under tensile testing, whereas AE distributions were rather closer under compressive tests, due to the difference in fracture energies between two tests. For both tests, carbon and basalt fiber breaks occurred around the yielding point. Beyond yielding much more AE events occurred from the interlayer failure in carbon fiber tensile cases, whereas basalt fiber did not exhibit such distinct interlayer signals. Ultimate stress in compressive loading exhibited much higher than that of tensile loading. The maximum AE voltage for the waveform of fiber breaks under tensile tests exhibited much larger than those under compressive tests.

ACKNOWLEDGEMENT This study was supported financially by KOSEF through the Research Center for Aircraft Parts Technology (ReCAPT), Gyeongsang National University.

REFERENCES

1. T. Grubb, and Z. F. Li, "Single-fiber polymer composites: Part I Interfacial shear strength and stress distribution in the pull-out test", Journal of Materials Science, Vol. 29, 1994, pp.189-202.

2. A. Kelly and W. R. Tyson, "Tensile properties of fiber reinforced metals: copper/tungsten and copper/molybdenum", Mech. and Phys. of Solids, Vol. 13, 1965, pp 329-350.

3. J. M. Park, S. I. Lee, D. W. Shin and D. J. Yoon, "Interfacial properties of glass fiber/brittle-ductile dual-matrix composites using micromechanical techniques and acoustic emission", Poly-

mer Composites, Vol. 20, 1999, pp.19-28.

4. J. M. Park, W. G. Shin, and D. J. Yoon, "Interfacial aspects of two basalt and SiC fiber reinforced epoxy composites using fragmentation technique and acoustic emission", Composites Science & Technology, Vol. 59, 1999, pp. 355-370.

5. D. B. Marshall and W. C. Oliver, "An introduction method for measuring residual stress in fiber reinforced ceramics", Materials Science and Engineering, Vol A 126, 1990, pp.95-103.

6. C. Ageorges, K. Friedrich, T. Schuller, and B. Lauke, "Single fiber Broutman test: fiber-matrix interface transverse debonding", Composites Part A, Vol. 30, 1999, pp. 1423-1434

7. J. R. Wood, H. D. Wagner, and G. Marom, "The compressive fragmentation phenomenon: using microcomposites to evaluate thermal stress, single fibre compressive strengths, Weibull parameters and interfacial shear strength", Proceeding of Royal Society London. A, 452, 1996, pp 235-252.

8. J. R. Wood, and G. Marom, "Determining the interfacial shear strength in the presence of transcrystallinity in composite by the 'single-fiber microcomposite compressive fragmentation test'", Applied Composites Materials, Vol. 4, 1997, pp. 117-124.

9. H. D. Wagner, C. Migliaresi, A. H. Gilbert, and G. Marom, "Transverse loading of monofilament reinforced microcomposites: a novel fragmentation technique for measuring the fiber compressive strength", Journal of Material Science, Vol. 27, 1992, pp. 4175-4180.

10. C. M. Ballie and M. G. Bader, "Some aspects of interface adhesion of electrolytically oxidized carbon fibers in an epoxy resin matrix", Journal of Material Science, Vol. 29, 1994, pp. 3822-3836.

11. Z. F. Li, A. N. Netravali, and W. Sachse, "Ammonia plasma treatment of ultra-high strength polyethylene fiber for improved adhesion to epoxy resin", Journal of Material Science, Vol. 27, 1992, pp. 4625-4632.

12. J. M. Park, "Interfacial aspects of two-carbon fiber reinforced polycarbonate composites using two-synthesized graft copolymers as coupling agents", Journal of Colloid and Interface Science, 2000 (in press).

13. J. M. Park, J. O. Lee, and C. W. Park, "Improvements of interfacial shear strength and durability in single carbon fibre reinforced isotactic polypropylene composites using water dispersible graft copolymer as a coupling agent", Polymer Composites, Vol. 17, 1996, pp. 375-383.

14. R. V. Subramanian, A. S. Crasto, "Electrodeposition of a polymer interphase in carbon-fiber composites", Polymer Composites, Vol. 7, 1986, pp. 201-218.

15. J. M. Park, Y. M. Kim, K. W. Kim, and D. J. Yoon, "Interfacial properties of electrodeposited carbon fibers reinforced epoxy composites using nomomeric and polymeric coupling", Journal of Colloid and Interface Science, 2000 (accepted).

16. J. M. Park, Y. M. Kim, K. W. Kim, and D. J. Yoon, "Interfacial properties of electrodeposited carbon fibers reinforced epoxy composites using fragmentation technique and acoustic emission", ICCE/6, 1999, pp. 645-646.

17. Q. Q. Li, and E. Jinen, "Fracture behavior and acoustic emission in bending tests on signle-fiber composites", Engineering Fracture Mechanics, Vol. 56, No.6, 1997, pp. 779-796.

18. A. N. Netravali, Z. F. Li, and W. Sachse, "Determination of fibre/matrix interfacial shear strength by an acoustic emission technique", Journal of Material Science, Vol. 26, 1991, pp. 6631-6638.

19. N. S. Choi, K. Takahasi and K. Hosino, "Characteristics of acoustic emission during the damage process in notched short-fiber-reinforced thermoplastics", NDT & E International, Vol. 25, 1992, pp.271-278.

20. N. S. Choi and K. Takahashi, "Characterization of the damage process in short-fiber/thermoplastic composites by acoustic emission", Journal

of Materials Science, Vol. 33, 1998, pp. 2357-2363.

21. H. F. Wu, A. N. Netravali, "Weibull analysis of strength-length relationships in single Nicalon SiC fibres", Journal of Materials Science, Vol. 27, 1992, pp.3318-3324.

22. K. Goda, J. M. Park, and A. N. Netravali, "A new theory to obtain Weibull fibre strength parameters from a single-fibre composite test", Journal of Materials Science, Vol. 30, 1995, pp.2722-1728.

23. T. Oshawa, M. Miwa, M. Kawade, & E. Tsutshima, "Axial compressive strength of carbon fibres" Journal of Applied Polymer Science, Vol. 39, 1990, pp.1733-1743.